

Bioinformatic and biochemical analysis of the key binding sites of the pheromone binding protein of *Cyrtotrachelus buqueti* Guerin-Meneville (Coleoptera: Curculionidea)

Hua Yang^{Equal first author, 1}, Yan-Lin Liu^{Equal first author, 1}, Yuan-Yuan Tao¹, Wei Yang^{Corresp., 1}, Chun-Ping Yang¹, Jing Zhang², Li-Zhi Qian¹, Hao Liu¹, Zhi-Yong Wang³

¹ Sichuan Agricultural University, Key Laboratory of Ecological Forestry Engineering of Sichuan Province/College of Forestry, Chengdu, Sichuan, China

² Provincial Key Laboratory of Agricultural Environmental Engineering, Sichuan Agricultural University, Chengdu, China

³ Key Laboratory of Control and Resource Development of Bamboo Pest of Sichuan Province, Leshan, China

Corresponding Author: Wei Yang

Email address: ywei0218@aliyun.com

The bamboo snout beetle *Cyrtotrachelus buqueti* is a widely distributed wood-boring pest found in China, and its larvae cause significant economic losses because this beetle targets a wide range of host plants. A potential pest management measure of this beetle involves regulating olfactory chemoreceptors. In the process of olfactory recognition, pheromone-binding proteins (PBPs) play an important role. Homology modeling and molecular docking were conducted in this study for the interaction between CbuqPBP1 and dibutyl phthalate to better understand the relationship between PBP structures and their ligands. Site-directed mutagenesis and binding experiments were combined to identify the binding sites of CbuqPBP1 and to explore its ligand-binding mechanism. The 3D structural model of CbuqPBP1 has six α -helices. Five of these α -helices adopt an antiparallel arrangement to form an internal ligand-binding pocket. When docking dibutyl phthalate within the active site of CbuqPBP1, a CH- π interaction between the benzene ring of dibutyl phthalate and Phe69 was observed, and a weak hydrogen bond formed between the ester carbonyl oxygen and His53. Thus, Phe69 and His53 are predicted to be important residues of CbuqPBP1 involved in ligand recognition. Site-directed mutagenesis and fluorescence assays with a His53Ala CbuqPBP1 mutant showed no affinity toward ligands. Mutation of Phe69 only affected binding of CbuqPBP1 to cedar camphor. Thus, His53(Between α 2 and α 3) of CbuqPBP1 appears to be a key binding site residue, and Phe69(Located at α 3) is a very important binding site for particular ligand interactions.

1 **Bioinformatic and biochemical analysis of the key binding sites of the**
2 **pheromone binding protein of *Cyrtotrachelus buqueti* Guerin-Meneville**
3 **(Coleoptera: Curculionidea)**

4 Hua Yang^{1¶}, Yan-Lin Liu^{1¶}, Yuan-Yuan Tao^{1¶}, Wei Yang^{1*}, Chun-Ping Yang¹, Jing Zhang², Li-
5 Zhi Qian¹, Hao Liu¹ and Zhi-Yong Wang³

6

7 ¹ Key Laboratory of Ecological Forestry Engineering of Sichuan Province, College of Forestry,
8 Sichuan Agricultural University, Chengdu, Sichuan 611130, China.

9 ² Provincial Key Laboratory of Agricultural Environmental Engineering, Sichuan Agricultural
10 University, Chengdu, Sichuan 611130, China.

11 ³ Key Laboratory of Control and Resource Development of Bamboo Pest of Sichuan Province,
12 Leshan, Sichuan, 614000, China.

13

14 *Corresponding Author:

15 Wei Yang

16 E-mail: ywei0218@aliyun.com

17 ¶These authors contributed equally to this article

19 **Abstract**

20 The bamboo snout beetle *Cyrtotrachelus buqueti* is a widely distributed wood-boring pest found
21 in China, and its larvae cause significant economic losses because this beetle targets a wide range
22 of host plants. A potential pest management measure of this beetle involves regulating olfactory
23 chemoreceptors. In the process of olfactory recognition, pheromone-binding proteins (PBPs)
24 play an important role. Homology modeling and molecular docking were conducted in this study
25 for the interaction between CbuqPBP1 and dibutyl phthalate to better understand the relationship
26 between PBP structures and their ligands. Site-directed mutagenesis and binding experiments
27 were combined to identify the binding sites of CbuqPBP1 and to explore its ligand-binding
28 mechanism. The 3D structural model of CbuqPBP1 has six α -helices. Five of these α -helices
29 adopt an antiparallel arrangement to form an internal ligand-binding pocket. When docking
30 dibutyl phthalate within the active site of CbuqPBP1, a CH- π interaction between the benzene
31 ring of dibutyl phthalate and Phe69 was observed, and a weak hydrogen bond formed between
32 the ester carbonyl oxygen and His53. Thus, Phe69 and His53 are predicted to be important
33 residues of CbuqPBP1 involved in ligand recognition. Site-directed mutagenesis and
34 fluorescence assays with a His53Ala CbuqPBP1 mutant showed no affinity toward ligands.
35 Mutation of Phe69 only affected binding of CbuqPBP1 to cedar camphor. Thus, His53(Between
36 α 2 and α 3) of CbuqPBP1 appears to be a key binding site residue, and Phe69(Located at α 3) is a
37 very important binding site for particular ligand interactions.

38 **Keywords:** *Cyrtotrachelus buqueti*, pheromone binding protein, bioinformatics, site-directed

39 mutagenesis, fluorescence assay

40

41 Introduction

42 During long-term evolution insects have developed a sensitive sense of smell, which enables
43 insects to detect external volatile semiochemicals when searching for various environmental cues,
44 such as foraging for food, finding a breeding partner and locating a spawning ground(Gu *et al.*,
45 2011; Larsson *et al.*, 2004). Tentacles are the main olfactory part of insects and contain a large
46 variety of receptors. Receptors are widely distributed with various olfactory-rated functional
47 proteins, including odorant binding proteins (OBPs), chemosensory proteins (CSPs) and
48 olfactory receptors (Ors). OBPs are divided into pheromone binding proteins (PBPs), general
49 odorant binding proteins (GOBPs) and antennal binding proteins (ABPs)(Vogt and Riddiford
50 1981). Research on the binding mechanism between OBPs and ligand molecules has been a
51 major focus of research, including defining the three-dimensional (3D) structure of these OBPs.
52 Kruse *et al.*, (2003) and Thode *et al.*, (2008) initially analyzed the general odorant binding
53 protein (LUSH) of *Drosophila melanogaster* and the crystal structure of the complex between
54 LUSH and alcohol, and clarified that Thr57 is a key residue involved in ligand interaction. In
55 accordance with X-ray diffraction analysis of the pheromone binding protein BmorPBP of
56 *Bombyx mori* and structure of bombykol, Sandler *et al.* (2000) discovered that Ser56 of this
57 protein played a key role by forming a hydrogen bond with the ligand bombykol. According to
58 the structures of odorant binding protein CquiOBP1 and MOP of *Culex quinquefasciatus*, Mao *et*
59 *al.* (2010) discovered that instead of hydrogen bonds, the interaction between protein and ligand
60 was driven by van der Waals forces and hydrophobic interactions. Based on the structure

61 between the odorant binding protein HoblOBP2 of *Holotrichia oblita* and ethyl
62 benzenecarboxylate, Zhuang *et al.* (2013) discovered that this protein-ligand complex involved
63 both van der Waals forces and hydrophobic interactions. Currently, high-resolution structural
64 data describing the complex between the pheromone binding protein of *Cyrtotrachelus buqueti*
65 and an odor molecule is unavailable, and thus information about the mode of action of this
66 protein remains unresolved.

67 *Cyrtotrachelus buqueti* (*C. buqueti*) also named as the bamboo snout beetle, belongs to
68 *Cyrtotrachelus*, Curculionidea, Coleoptera. *C. buqueti* is endangering survival of bamboo shoots
69 from 28 different types of bamboos, including *Bambusa*, *Dendrocalamopsis* and *Dendrocalamus*.
70 In particular, the larvae prefer the bamboo shoots of *Phyllostachys pubescens*,
71 *Dendrocalamopsis oldhami*, *Bambusa textilis*, *Bambusa pervariabilis*, *Dendrocalamopsis daii*
72 and other sympodial bamboo species(Ju *et al.*, 2005; Wang *et al.*, 2005). *C. buqueti* is distributed
73 widely in the Sichuan Province, Chongqing City, Guangdong Province, Guangxi Province,
74 Guizhou Province and other provinces (districts) as well as Vietnam, Burma, Thailand and other
75 countries and regions in Southeast Asia(Yang *et al.*, 2009). *C. buqueti* is one of 233 hazardous
76 forest pests issued in 2003 for the first time(Yang *et al.*, 2015).

77 Currently, research on *C. buqueti* has mainly concentrated on a description of the general
78 biological characteristics and common chemical pest control approaches(Ju *et al.*, 2005; Wang *et*
79 *al.*, 2005; Yang *et al.*, 2010; Yang *et al.*, 2009). The development of sex attractants remains
80 poorly understood. Mang *et al.* (2012) have extracted and studied the body surface

81 semiochemicals of *C. buqueti* adults, whereas Yang *et al.* (2017a) have constructed a
82 transcriptome library of *C. buqueti* and analyzed the sex pheromone binding protein gene. Yang
83 *et al.* (2017b) have also cloned the sex pheromone binding protein gene that codes for the protein
84 CbuqPBP1, and conducted fluorescence competitive binding assays for many types of simple
85 odor substances. Based on a phylogenetic analysis (Yang *et al.*, 2018; summarized in
86 supplementary information) CbuqPBP1 was quite similar to the PBPs of other insects. Amino
87 acid sequence similarity analysis showed that CbuqPBP1 had 37.68% similarity with 27 PBPs of
88 17 insects of Coleoptera and Lepidoptera. The similarities with PBPs from Coleoptera and
89 Lepidoptera were 38.47% and 52.39% respectively.

90 In this paper, homology modeling of the pheromone binding protein CbuqPBP1 of *C.*
91 *buqueti* has been conducted to create a 3D model of the protein. Molecular docking has also been
92 carried out to define the interaction mode between the ligand dibutyl phthalate and CbuqPBP1.
93 Two key binding site residues, Phe69 and His53, were identified from this modeling and were
94 mutated. Fluorescence competitive binding assays were conducted for these mutants and binding
95 mechanism between CbuqPBP1 and odor molecules was analyzed. The results provide a
96 platform for using pheromones to prevent and control *C. buqueti* efficiently.

97

98 **Materials & Methods**

99 **Materials**

100 Three compounds were chosen to investigate the ligand-binding specificity of CbuqPBP1.
101 Ligands of the highest purity were purchased from Aladdin (Shanghai, China) and stored in
102 accordance with the manufacture's specifications. The sequence of CbuqPBP1 was taken from
103 the GenBank with accession number KU845733.1.

104 **Alignment and homology modeling**

105 The amino acid sequence of CbuqPBP1 was downloaded from the GenBank and Blast was used
106 to search against the CbuqPBP1 protein sequence in the Protein Data Bank to identify a
107 structural template. Software Modeller 9.19 (<http://salilab.org/modeller/>) was used for homology
108 modeling based on the sequence comparison results with the structural template sequence
109 identified. The 3D structure obtained from modeling was evaluated with SAVES v5.0
110 (<https://servicesn.mbi.ucla.edu/SAVES/>). After confirming the models, the Chiron
111 (<http://redshift.med.unc.edu/chiron/login.php>) on-line server was used for optimization. Modeller
112 9.19 was used to optimize loop regions and PyMOL was used to analyze structural
113 characteristics and to search for ligand binding sites.

114 **Molecular docking**

115 Based on the established homology model, the docking program AUTODOCK vina 1.1.2 was
116 used to find the potential binding mode between CbuqPBP1 and the ligand dibutyl phthalate.
117 Dibutyl phthalate with strong affinity is a female pheromone of the giant bamboo weevil, which
118 plays a role in the process of male individual searching for female individual. ChemBioDraw

119 Ultra 14.0 was used to simulate the structure of dibutyl phthalate and to generate a 3D structure
120 of the ligand. Energy optimization was conducted using the MMFF94 force field and Autodock
121 Tools 1.5.6 was used to create the PDBQT format(Huey *et al.*, 2007; Morris *et al.*, 2009).
122 Binding coordinates of CbuqPBP1 and dibutyl phthalate were set to: center_x = 22.389, center_y
123 = -25.143, center_z = 1.08, and size_x = 15, size_y = 15, size_z = 15. Parameter exhaustiveness
124 was set to 20 and default values were used for other parameters to increase the calculation
125 accuracy. Finally, the conformation with the highest score was selected and PyMoL 1.7.6 was
126 used for visual inspection and analysis of the structural data.

127 **Site-directed mutagenesis**

128 The CbuqPBP1 coding sequence was mutated to yield the two mutants CbuqPBP1-Phe69A
129 (phenylalanine to alanine at position 69) and CbuqPBP1-His53A (histidine to alanine at position
130 53). PCR reactions were used to form overlapping chains. The extension of overlapping chains
131 was used to splice segments in a superimposed manner. Primer5 was used to design primers
132 (Table 1). Three rounds of PCR amplification were conducted after designing primers.
133 Expression vectors (pET-28a+)/PBP1-Phe69A, pET-28a+)/PBP1-His53A and pET-
134 28a+)/PBP1) were generated and transformed into *Escherichia coli* BL21(DE3) competent cells
135 for protein overexpression. Recombinant proteins produced were detected by SDS-PAGE
136 analysis.

137 **Expression and purification of the native protein and mutants**

138 Expression plasmids were transformed into *E. coli* TOP10 competent cell and plated on agar
139 plates. Several colonies were selected randomly for overnight cultivation in LB media and
140 plasmids were extracted for sequencing. Mutant plasmids pET-28a(+)/PBP1- Phe69A and pET-
141 28a(+)/PBP1- His53A with the correct sequence were transformed into *E. coli* BL21(DE3)
142 competent cells, and cells were grown to an optical density at 600 nm (OD₆₀₀) of 0.6. IPTG was
143 added to the culture to a final concentration of 1 mM and cells were further grown at 37 °C with
144 shaking for 3 h to induce protein expression(Deng *et al.*, 2011). After harvesting cells by
145 centrifugation, ultrasound sonication was used to disrupt cells (200 W, 3/4 s, 25–30 min). The
146 supernatants and sediments were collected under low temperature centrifugation (16000 g-force,
147 50 min) and SDS-PAGE detection was conducted. Nickel affinity (Ni-NTA) was used to purify
148 recombination proteins, and the purified proteins were stored in Tris-HCl buffer (pH 7.4, 50
149 mM). To avoid the function of the protein being affected by the His-tag, recombinant bovine
150 enterokinase was used to remove the His-tag and the protein was re-purified and collected. Purity
151 was confirmed by SDS-PAGE analysis.

152 **Fluorescence assay**

153 To measure the affinity of the fluorescent ligand N-phenyl-1-naphthylamine (1-NPN) toward
154 CbuqPBP1, a 2 μM solution of protein in 50 mM Tris-HCl, pH 7.4, was titrated with aliquots of
155 1 mM 1-NPN dissolved in methanol to a final concentration of 16 μM. The probe was excited at
156 337 nm and emission spectra were recorded between 350 and 550 nm. To evaluate the effect of
157 pH on the binding affinity of CbuqPBP1, we also measured its binding with 1-NPN over a pH

158 range of 4.5–9.0. The displacement of 1-NPN by selected ligands was measured in a competitive
159 binding assay using both the protein and 1-NPN at 2 μM . The mixtures were titrated with 1 mM
160 methanol solutions of each competitor at concentrations of 2–16 μM . The fluorescence of the
161 mixture was recorded after 5 min. Dissociation constants for 1-NPN and the stoichiometry of
162 binding were obtained from Scatchard plots of the binding data using the Prism software. For
163 other competitor ligands, the dissociation constants were calculated from the corresponding half
164 maximal inhibitory concentration (IC_{50}) values using the equation: inhibitory constant $K_i =$
165 $[\text{IC}_{50}]/(1 + [1\text{-NPN}]/K_{1\text{-NPN}})$, where [1-NPN] is the free concentration of 1-NPN and $K_{1\text{-NPN}}$ is the
166 dissociation constant of the protein/1-NPN complex.

167

168 **Results**

169 **Three-dimensional model of CbuqPBP1**

170 On the basis of the Blast search against the Protein Data Bank, two types of insect odor proteins
171 with known structures and quite similar sequences to the CbuqPBP1 sequence were found. These
172 two odorant binding proteins were *Nasonovia ribisnigri* OBP3 (NribOBP3 PDB ID: 4Z45_A)
173 and *Megoura viciae* OBP3 (MvicOBP3 PDB ID: 4Z39_A). The total sequence identity between
174 the target (CbuqPBP1) and the template protein (NribOBP3) is 33% (Cavasotto and Phatak
175 2009)(Fig. 1A). The resolution of the template is 2.02 Å.

176 After homology modeling, the 3D structure of CbuqPBP1 (Fig. 1B) is clearly very similar

177 to the 3D structure of the template NribOBP3 (Fig. 1C). The structural characteristics of
178 CbuqPBP1 are similar to other sex pheromone binding proteins and include six α -helices:
179 residues 26–36 (α 1), 44–51 (α 2), 59–72 (α 3), 83–94 (α 4), 101–114 (α 5) and 123–137 (α 6). Six
180 conserved cysteine residues stabilize the protein structure by forming three disulfide bonds.
181 Disulfide bond Cys36–Cys67 connects α 1 and α 3, Cys63–Cys121 connects α 3 and α 6, and
182 Cys110–Cys130 connects α 5 and α 6. Five of the α -helices adopt an antiparallel arrangement
183 (α 1, α 3, α 4, α 5 and α 6) and form an internal binding pocket. α 2 forms a cover-type structure or
184 lid above the pocket, which stabilizes this structure.

185 The result of further rationality estimates by Pro-CHECK (Fig. 1D) was that 88.4% residues
186 were in the favored regions (red area A, B and L), 10.1% of the residues fall into additionally
187 allowed regions (bright yellow area a, b, l, p) and 0.8% residues have backbone torsion angles
188 that fall into generously allowed regions (light yellow area \sim a, \sim b, \sim l, \sim p). The percentage sum
189 of residues in the allowed regions was 99.3%, which was higher than 95%. This result showed
190 that the constructed 3D structure of CbuqPBP1 was a high-quality model.

191 Energy assessment was performed on ProSa (Fig. 1E). The shadow part is Z-score value
192 of all proteins similar to Cbuq PBP1 protein in PDB database, and the black spot is Z-score value
193 of Cbuq PBP1 protein, which is -4.35. The Z-score value of template protein NOBP3 is -5.87 in
194 the range of Z-score of known reasonable structural proteins, which indicates that the modeling
195 structure is more stable than template structure. This indicates that the homologous modeling
196 Institute is more stable than template structure. The constructed CBUq PBP1 protein is

197 reasonable in energy.

198 **Molecular docking**

199 To research characteristics of CbuqPBP1 binding with odor molecules, dibutyl phthalate
200 (Fig. 2A), which interacts with CbuqPBP1 favorably, was selected to construct a complex
201 between CbuqPBP1 3D model and dibutyl phthalate. Such a model should clarify the mode of
202 interaction of dibutyl phthalate with CbuqPBP1 at the molecular level. We have docked dibutyl
203 phthalate with the active pocket of CbuqPBP1, with a binding energy of -6.4 kcal/mol.
204 Generally, compound dibutyl phthalate bound to the active pocket of CbuqPBP1 with a compact
205 conformation (Fig. 2B).

206 The benzene ring and one aliphatic chain of dibutyl phthalate were located in the
207 hydrophobic region at the bottom of the pocket. Strong hydrophobic interactions formed between
208 the ligand and residues Leu3, Leu4, Leu5, Leu29, Leu50, Pro56, Ile65 and Phe69. Another side
209 chain of dibutyl phthalate was located at the opening of the pocket. Based on detailed analysis, a
210 CH- π interaction may occur between the benzene ring of dibutyl phthalate and residue Phe69.
211 Moreover, an important long-range hydrogen bond (3.3 Å) can form between one ester carbonyl
212 oxygen of dibutyl phthalate and residue His53 (Fig. 2C). All aforementioned interactions enable
213 the formation of a stable complex between dibutyl phthalate and CbuqPBP1.

214 **Site-directed mutagenesis of CbuqPBP1 and binding specificities of mutants**

215 After double enzyme digestion with restriction enzymes *Nde* I and *Xha* I, mutant plasmids pET-

216 28a(+)/CbuqPBP1-His53A and pET-28a(+)/CbuqPBP1-Phe69A, and the original plasmid pET-
217 28a(+)/PBP1 formed bands in an agarose gel that were ~400 bp in length (Fig. 3). After SDS-
218 PAGE analysis of protein overexpression, three specific bands with molecular weights of 16 kDa
219 were observed in the SDS-PAGE gel, which is consistent with expected molecular weight of the
220 target proteins (Fig. 4).

221 After ultrasonication to disrupt the bacteria and release the recombinant proteins (including
222 His tag), SDS-PAGE analysis could be conducted (Fig. 5). All recombinant proteins were found
223 in the supernatant part of the disrupted cells. After purification, recombinant bovine enterokinase
224 was used to cleave the His-tag and following a further round of purification pure recombinant
225 protein samples were obtained.

226 1-NPN was selected as the fluorescent probe. Fluorescence competitive binding assays were
227 conducted for the purified wild-type CbuqPBP1, mutant CbuqPBP1-His53A and CbuqPBP1-
228 Phe69A proteins. The fluorescence peak maximum in the presence of the recombinant proteins
229 was recorded at different concentrations. The Scatchard equation was used to calculate the
230 equilibrium binding constant (K_d) between CbuqPBP1, CbuqPBP1-His53A, CbuqPBP1-Phe69A
231 and 1-NPN, which were determined to be 2.725, 3.352 and 2.260 μM , respectively. When the
232 final concentration of odor substance was higher than 50 μM , the fluorescence peak did not
233 decrease to half its value. This showed that almost no affinity was established between protein
234 and the odor substance, and the binding constant could not be calculated (Fig. 6).

235 Dibutyl phthalate, benzothiazole and cedar camphor were selected based on previous

236 fluorescence binding assay test(Yang *et al.*, 2017b). Fluorescence competitive binding assays
237 were conducted with CbuqPBP1, CbuqPBP1-His53A and CbuqPBP1-Phe69A (Fig. 7). Based on
238 the results, CbuqPBP1 bound favorably with dibutyl phthalate, benzothiazole and cedar camphor.
239 The binding ability of CbuqPBP1-His53A with the three types of odor substances was essentially
240 lost. The binding ability of CbuqPBP1-Phe69A mutant with cedar camphor was significantly
241 reduced, whereas affinity toward the other two odor substances was not significantly different
242 from that of the wild-type protein (Table 2).

243

244 **Discussion**

245 Currently, 3D structure prediction of odorant binding proteins through homology modeling has
246 been conducted for proteins from *Choristoneura rosaceana*, *Choristoneura murinana*,
247 *Pectinophora gossypiella*, *Heliothis assulta*, *Spodoptera exigua*, *Spodoptera exigua*, *Holotrichia*
248 *oblita*, *lettuce Aphidoidea*, *Megoura viciae* and other insects(Northey *et al.*, 2016; Sun *et al.*,
249 2013; Wang *et al.*, 2015). On the basis of homology modeling of pheromone binding protein
250 CbuqPBP1 of *C. buqueti*, the 3D structure is composed of six α -helices, which packed together
251 and were stabilized by three disulfide bonds. Disulfide bonds Cys36–Cys67, Cys63–Cys121 and
252 Cys110–Cys130 connected α 1 and α 3, α 3 and α 6, α 5 and α 6 respectively. Five of the α -helices
253 arranged in an antiparallel manner to form an internal binding pocket(Tian *et al.*, 2017). α 2
254 formed a cover-type structure above the pocket, which was similar to *Holotrichia oblita*
255 HoblOBP2(Zhuang *et al.*, 2013) structures. As for 3D structure of *Bombyx mori* BmorPBP, four

256 antiparallel α -helices formed a hydrophobic pocket and $\alpha 2$ and $\alpha 3$ did not participate in the
257 formation of the pocket(Sandler *et al.*, 2000). This might be due to differences in hydrophobic
258 pocket of the 3D structure of odorant binding proteins from different insects. Such differences
259 are likely to be closely related to the function of these proteins.

260 According to research, odorant binding proteins from some insects interact with their cognate
261 ligand through hydrogen bonds and hydrophobic interactions, whereas other odorant binding
262 proteins from other insects interact with odorants via van der Waals forces and hydrophobic
263 interactions(Sandler *et al.*, 2000). In this report, a CH- π interaction formed between the benzene
264 ring of dibutyl phthalate and Phe69. This CH- π interaction is generally considered to be a
265 relatively weak hydrogen bond. Previous research has indicated that CH- π interactions are
266 important in carbohydrate–protein identification processes, where the CH- π features as a
267 synergistic interaction that plays an important role in stabilizing the structure of the complex
268 (Jiang *et al.*, 2009; Kozmon *et al.*, 2011). The CH- π interaction involves a nonpolar interaction
269 between the CH proton and electron-rich aromatic ring π electron cloud system, playing a similar
270 role to hydrogen bonding in controlling crystal stacking, maintaining biomolecular structures and
271 participating in molecular recognition processes(Ye *et al.*, 2015; Zhao *et al.*, 2014). Therefore,
272 we hypothesize that the CH- π interaction may play a role in binding and stabilizing the
273 interaction with odor molecules.

274 An ester carbonyl oxygen from dibutyl phthalate and His53 from the protein formed a weak
275 3.3 Å hydrogen bond. Such a hydrogen bond has been reported in odorant binding proteins of

276 other insects, for example, BmorPBP1 of *B. mori* and pheromone compound interacted through a
277 hydrogen bond. General odorant binding protein (LUSH) from *Drosophila melanogaster* and the
278 pheromone binding protein (ApolPBP1) from *Antheraea polyphemus* interact with their cognate
279 ligands through hydrogen bonds(Damberger *et al.*, 2007; Thode *et al.*, 2008).

280 According to the fluorescence competitive binding assay, mutant pET-28a(+)/PBP1-His53A
281 could not interact with odor substances. Replacing His53 with alanine removed the ability of the
282 mutant to form this key hydrogen bond with ligands, and therefore the ability to bind with odor
283 substances. Thus, His53 is a key binding site residue of the pheromone binding protein of *C.*
284 *buqueti*. Mutein pET-28a(+)/PBP1-Phe69A did not bind cedar camphor. However, only a
285 decrease in binding ability toward dibutyl phthalate and benzothiazole was observed. These
286 observations indicate that only a small number of intermolecular forces between the protein and
287 odor molecules were affected by this mutation(Zhuang *et al.*, 2014). Thus, the binding affinity
288 had been reduced, but not completely lost.

289 **Conclusions**

290 In summary, we hypothesized that the CbuqPBP1 interaction and release of the ligand involves
291 hydrogen bond formation via His53. Phe69 is the binding site for CbuqPBP1 to combine with
292 odor substance; however, Phe69 is not a key binding site residue. Moreover, these observations
293 showed that the combination between CbuqPBP1 and ligands was affected by loss of hydrogen
294 bonding and other intermolecular forces, and the interaction between CbuqPBP1 and ligands
295 involves the joint action of many acting forces and the binding site(Li et al. 2016).

296 Acknowledgments

297 This work was funded by the key fund of the education department in Sichuan (17ZB0344) and
298 the key laboratory fund for scientific research in Sichuan (003Z1401). The experiments were
299 conceived and coordinated by HY, YYT, YLL, WY, ZYW ,LZQ and CPY. Sampling was
300 performed by HY, YLL and YYT. Molecular docking was performed by HY, YLL, HL and JZ.
301 HY, YLL and WY drafted the manuscript. All authors read and approved the final version of the
302 manuscript submitted for publication. The authors thank Liwen Bianji, Edanz Editing China
303 (www.liwenbianji.cn/ac), for editing the English text of a draft of this manuscript.

304

305 **Figure legends**

306 **Figure 1 Three-dimensional (3D) model of CbuqPBP1.** (A) Sequence alignment between
307 CbuqPBP1 and NribOBP3. (B) 3D structure of CbuqPBP1. The N and C termini and the six α -
308 helices are labeled and the three disulfide linkages are shown in yellow stick representations. (C)
309 Superimposed penetrative structure of CbuqPBP1 and NribOBP3. The model of CbuqPBP1 and
310 crystal structure of NribOBP3 are shown in green and violet, respectively. (D) The results of the
311 PROCHECK evaluation of the CbuqPBP1 model. (E) Overall model quality.

312 **Figure 2 The binding pocket of CbuqPBP1 and the docking result with dibutyl phthalate.**
313 (A) Tertiary structure of dibutyl phthalate. (B) The binding pocket of CbuqPBP1 and dibutyl
314 phthalate docked into the active site of the CbuqPBP1 receptor. (C) Diagram of the van der
315 Waals interactions and hydrophobic interactions of dibutyl phthalate with key binding site
316 residues.

317 **Figure 3 Double digestion map of the mutant and wild-type plasmids.** Lane Marker: protein
318 molecular weight standard; Lane 1: pET-28a (+)/PBP1-Phe69A; Lane 2: pET-28a (+)/PBP1-
319 His53A; and Lane 3: pET-28a (+)/PBP1.

320 **Figure 4 SDS-PAGE analysis of the total bacterial protein lysate of the mutant and wild-**
321 **type CbuqPBP1.** (A) CbuqPBP1-His53A mutant. Lane 1: IPTG induced total protein lysate;
322 Lane 2: total protein lysate without IPTG induction. (B) CbuqPBP1- Phe69A mutant. Lane 1:
323 total protein lysate without IPTG induction; Lane 2: IPTG induced total protein lysate. (C) wild-

324 type CbuqPBP1. Lane 1: IPTG induced total protein lysate; Lane 2: total protein lysate without
325 IPTG induction.

326 **Figure 5 SDS-PAGE analysis of supernatant and precipitant of bacterial fragmentation**
327 **following expression of the mutant and wild-type CbuqPBP1.** Lane 1: IPTG induced
328 expression of insoluble material; Lane 2: IPTG induced expression of supernatant following cell
329 disruption by sonication. (A) wild-type protein. (B) CbuqPBP1-His53A mutant. (C) CbuqPBP1-
330 Phe69A mutant.

331 **Figure 6 The binding curve and K_d of mutant and wild-type CbuqPBP1 toward 1-NPN.** (A)
332 wild-type protein. (B) CbuqPBP1-His53A mutant. (C) CbuqPBP1- Phe69A mutant.

333 **Figure 7 Competitive binding curves of selected ligands toward mutant and wild-type**
334 **CbuqPBP1.** (A) wild-type protein. (B) CbuqPBP1-His53A mutant. (C) CbuqPBP1- Phe69A
335 mutant.

336

337 Reference

338 Cavasotto, C.N., and S.S. Phatak. 2009. Homology modeling in drug discovery: current trends and applications.
339 Drug Discov Today 14: 676-683.

340 Damberger, F.F., Y. Ishida, W.S. Leal and K. Wuthrich. 2007. Structural basis of ligand binding and release in insect
341 pheromone-binding proteins: NMR structure of *Antheraea polyphemus* PBP1 at pH 4.5. J Mol Biol 373: 811-819.

342 Deng, S.S., J. Yin, T. Zhong and Y.Z. Cao. 2011. Function and immunocytochemical localization of two novel
343 odorant-binding proteins in olfactory sensilla of the scarab beetle *Holotrichia oblita* Faldermann (Coleoptera:
344 Scarabaeidae). Chemical Senses 37: 141-150.

- 345 Gu, S.H., S.P. Wang, X.Y. Zhang, K.M. Wu, Y.Y. Guo, J.J. Zhou and Y.J. Zhang. 2011. Identification and tissue
346 distribution of odorant binding protein genes in the lucerne plant bug *Adelphocoris lineolatus* (Goeze). *Insect*
347 *Biochem Mol Biol* 41: 254-263.
- 348 Huey, R., G.M. Morris, A.J. Olson and D.S. Goodsell. 2007. A semiempirical free energy force field with charge-
349 based desolvation. *J Comput Chem* 28: 1145-1152.
- 350 Jiang, Q.Y., W.X. Wang, Z. Zhang and L. Zhang. 2009. Binding specificity of locust odorant binding protein and its
351 key binding site for initial recognition of alcohols. *Insect Biochem Mol Biol* 39: 440-447.
- 352 Ju, R.T., C.H. Xiao, J.H. Xu, Y. Xu, X.Z. Chi and Y.Z. Li. 2005. *Cyrtotrachelus buqueti* in Shanghai. *Forest Pest and*
353 *Disease* 24: 7-9.
- 354 Kozmon, S., R. Matuska, V. Spiwok and J. Koca. 2011. Dispersion interactions of carbohydrates with condensate
355 aromatic moieties: theoretical study on the CH- π interaction additive properties. *Phys Chem Chem Phys* 13:
356 14215-14222.
- 357 Kruse, S.W., R. Zhao, D.P. Smith and D.N. Jones. 2003. Structure of a specific alcohol-binding site defined by the
358 odorant binding protein LUSH from *Drosophila melanogaster*. *Nat Struct Biol* 10: 694-700.
- 359 Larsson, M.C., A.I. Domingos, W.D. Jones, M.E. Chiappe, H. Amrein and L.B. Vosshall. 2004. Or83b encodes a
360 broadly expressed odorant receptor essential for *Drosophila* olfaction. *Neuron* 43: 703-714.
- 361 Li, Y.H., P.Y. Deng, Y.M. Liu and Z.H. Lei. 2016. Binding mechanisms of sex pheromone with pheromone binding and
362 receptor proteins in *Plutella xylostella*. *Journal of Southern Agriculture* 47: 928-933.
- 363 Mang, D.Z., Q.H. Luo, M. Shu and W. Wei. 2012. Extraction and identification of cuticular semiochemical
364 components of *Cyrtotrachelus buqueti* Guerin-Meneville (Coleoptera: Curculionidae). *Acta Entomol Sin* 55: 291-302.
- 365 Mao, Y., X. Xu, W. Xu, Y. Ishida, W.S. Leal, J.B. Ames and J. Clardy. 2010. Crystal and solution structures of an
366 odorant-binding protein from the southern house mosquito complexed with an oviposition pheromone. *Proc Natl*
367 *Acad Sci U S A* 107: 19102-19107.
- 368 Morris, G.M., R. Huey, W. Lindstrom, M.F. Sanner, R.K. Belew, D.S. Goodsell and A.J. Olson. 2009. AutoDock4 and
369 AutoDockTools4: Automated docking with selective receptor flexibility. *J Comput Chem* 30: 2785-2791.
- 370 Northey, T., H. Venthur, F. De Biasio, F.X. Chauviac, A. Cole, K.A.J. Ribeiro, G. Grossi, P. Falabella, L.M. Field, N.H.
371 Keep and J.J. Zhou. 2016. Crystal Structures and Binding Dynamics of Odorant-Binding Protein 3 from two aphid
372 species *Megoura viciae* and *Nasonovia ribisnigri*. *Sci Rep* 6: 24739.
- 373 Sandler, B.H., L. Nikonova, W.S. Leal and J. Clardy. 2000. Sexual attraction in the silkworm moth: structure of the

- 374 pheromone-binding-protein-bombykol complex. *Chem Biol* 7: 143-151.
- 375 Sun, H., L.X. Zhao, F.R. Zhou and H. Gao. 2013. Pheromone binding protein of *Helicoverpa zea* based on Homology
376 modeling. *Ningxia Journal of Agriculture and Forestry Science and Technology* 54: 37-39.
- 377 Thode, A.B., S.W. Kruse, J.C. Nix and D.N. Jones. 2008. The role of multiple hydrogen bonding groups in specific
378 alcohol binding site in protein: Insights from structural studies of LUSH. *Journal of Molecular Biology* 376: 1360-
379 1376.
- 380 Tian, Z.Q., L.N. Sun, Y.Y. Li, H.J. Zhang, W.T. Yan, Q. Yue, L.F. Quan and G.S. Qiu. 2017. Research progress of the
381 function of sex pheromone binding protein in insects. *Journal of Agriculture* 7: 14-20.
- 382 Vogt, R.G., and L.M. Riddiford. 1981. Pheromone binding and inactivation by moth antennae. *Nature* 293: 161-163.
- 383 Wang, W.D., F.Z. Chen and X.Q. Wang. 2005. Reproductive behavior of *Cyrtotrachelus buqueti*. *Sichuan J Zool* 24:
384 540-541.
- 385 Wang, Y., H. Sun, J.Y. Zhu, N. Zhao and B. Yang. 2015. Homology modeling of the odorant binding protein of the
386 pine shoot beetle, *Tomicus yunnanensis*. *Chinese Journal of Applied Entomology* 54: 1223-1228.
- 387 Yang, H., T. Su, W. Yang, C. Yang, L. Lu and Z. Chen. 2017a. The developmental transcriptome of the bamboo snout
388 beetle *Cyrtotrachelus buqueti* and insights into candidate pheromone-binding proteins. *PLoS One* 12: e0179807.
- 389 Yang, H., T. Su, W. Yang, C.P. Yang, Z.M. Chen, L. Lu, Y.L. Liu and Y.Y. Tao. 2017b. Molecular characterization,
390 expression pattern and ligand-binding properties of the pheromone-binding protein gene from *Cyrtotrachelus*
391 *buqueti*. *Physiol Entomol* 42: 1-10.
- 392 Yang, H., T. Su, W. Yang, C.P. Yang, X.L. Zhou and Y. P. Li 2018. Molecular Cloning and Expression Analysis of
393 CbuqPBP1 Gene in the Bamboo Snout Beetle, *Cyrtotrachelus buqueti*. *Journal of Sichuan Agricultural University*
394 36:78-85.
- 395 Yang, H., W. Yang, C.P. Yang, Y. Cai, Y.F. Pu, Y.W. Fu and Z.R. He. 2015. Mating behavior of *Cyrtotrachelus buqueti*
396 (Coleoptera: Curculionidae). *Acta Entomol Sin* 58: 60-67.
- 397 Yang, Y.J., H. Qin, S.F. Wang, Y.P. Wang, H. Liao and S.G. Li. 2010. Antennal ultrastructure and electroantennogram
398 responses of *Cyrtotrachelus buqueti* Guerin-Meneville (Coleoptera: Curculionidae) to volatiles of bamboo shoot.
399 *Acta Entomol Sin* 53: 1087-1096.
- 400 Yang, Y.J., S.F. Wang, J.W. Gong, C. Liu, C. Mu and H. Qin. 2009. Relationships among *Cyrtotrachelus buqueti* larval
401 density and wormhole number and bamboo shoot damage degree. *Chinese J Appl Ecol* 20: 1980-1985.
- 402 Ye, Y.X., J.J. Liang, H.P. Wang, Z. Meng, X.D. Zhang and L.X. Xu. 2015. Noncovalent surface functionalization of

403 multi-walled carbon nanotubes with polyhedral oligomeric silsesquioxane nanoparticles based on CH- π
404 interactions. Acta Polymerica Sinica 4: 427-436.

405 Zhao, C., P. Li, M.D. Smith, P.J. Pellechia and K.D. Shimizu. 2014. Experimental study of the cooperativity of CH- π
406 interactions. Org Lett 16: 3520-3523.

407 Zhuang, X., Q. Wang, B. Wang, T. Zhong, Y. Cao, K. Li and J. Yin. 2014. Prediction of the key binding site of odorant-
408 binding protein of *Holotrichia oblita* Faldermann (Coleoptera: Scarabaeida). Insect Mol Biol 23: 381-390.

409 Zhuang, X.J., J. Yin, K.B. Li and Y.Z. Cao. 2013. Bioinformatics analysis of the odorant-binding protein HobLOBP2 in
410 olfactory sesilla of the scarab beetle *Holotrichia oblita*. Plant Protection 39: 50-55.

411

412

Table 1 (on next page)

Mutagenic primers for CbuqPBP1

| Primers | Sequence |
|--------------|--------------------------------------------------|
| PBP1-F69A-Fm | 5'-aatgcactatctgtacagcgaaaaattcgattgatgaaag-3' |
| PBP1-F69A-Rm | 5'-ctttcatcaaatcgaatcttcgctgtacagaaaatagtcatt-3' |
| PBP1-H53A-Fm | 5'-gatatccaagctctgatgaacggaacgaccagtcacccatgc-3' |
| PBP1-H53A-Rm | 5'-gcatgggtgactggcgtccggttcacagagcttgatc-3' |
| PBP1-F | 5'-ggaattccatagcttagcgaagcttagttgtgatg-3' |
| PBP1-R | 5'-ccgctcgagttaaaaactgtaattccaag-3' |

1

2

Table 2 (on next page)

Binding ability of ligands to mutant and wild-type CbuqPBP1

| Ligands | IC50 (μM) | | | Ki (μM) | | |
|-------------------|------------------------|------|--------|----------------------|------|--------|
| | PBP1 | H53A | F69A | PBP1 | H53A | F69A |
| benzothiazole | 13.426 | – | 10.538 | 9.822 | – | 7.305 |
| dibutyl phthalate | 16.889 | – | 20.04 | 12.355 | – | 13.893 |
| cedrol | 29.953 | – | – | 21.912 | – | – |

1

2

Figure 1

Three-dimensional (3D) model of CbuqPBP1

(A) Sequence alignment between CbuqPBP1 and NribOBP3. (B) 3D structure of CbuqPBP1. The N and C termini and the six α -helices are labeled and the three disulfide linkages are shown in yellow stick representations. (C) Superimposed penetrative structure of CbuqPBP1 and NribOBP3. The model of CbuqPBP1 and crystal structure of NribOBP3 are shown in green and violet, respectively. (D) The results of the PROCHECK evaluation of the CbuqPBP1 model. (E) Overall model quality.

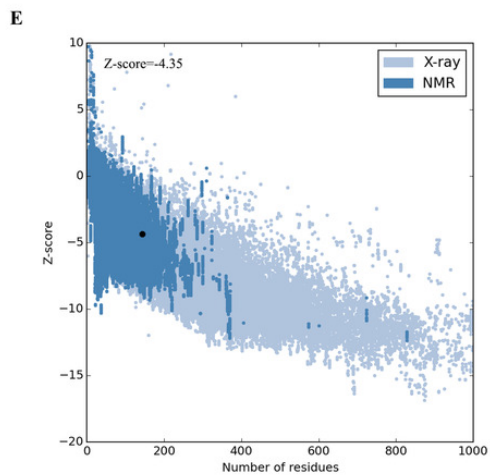
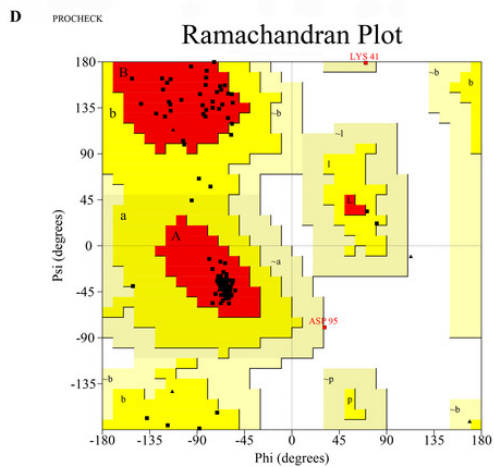
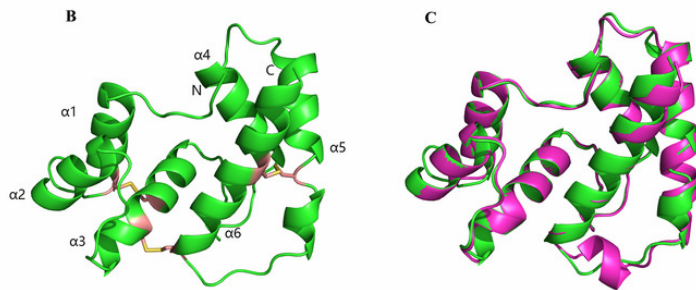
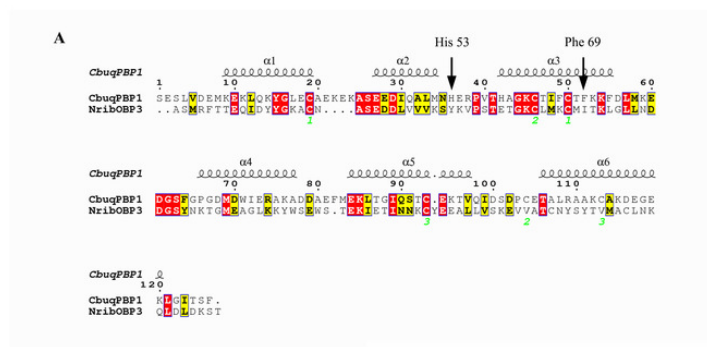
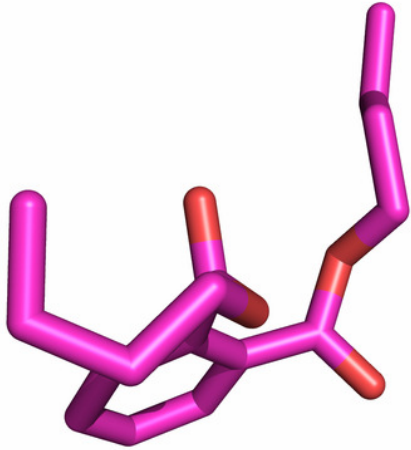


Figure 2

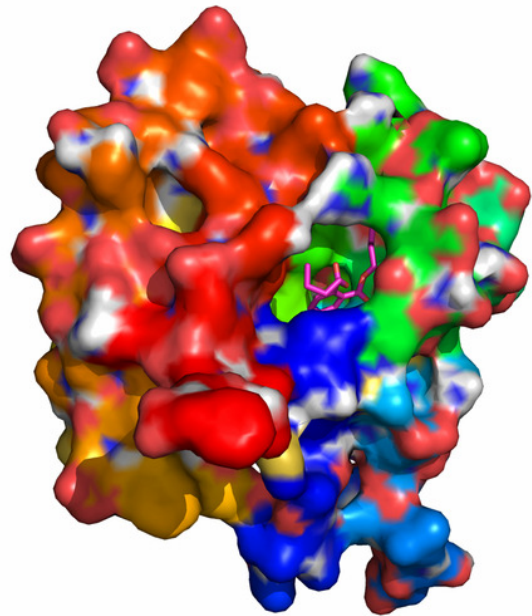
The binding pocket of CbuqPBP1 and the docking result with dibutyl phthalate

(A) Tertiary structure of dibutyl phthalate. (B) The binding pocket of CbuqPBP1 and dibutyl phthalate docked into the active site of the CbuqPBP1 receptor. (C) Diagram of the van der Waals interactions and hydrophobic interactions of dibutyl phthalate with key binding site residues.

A



B



C

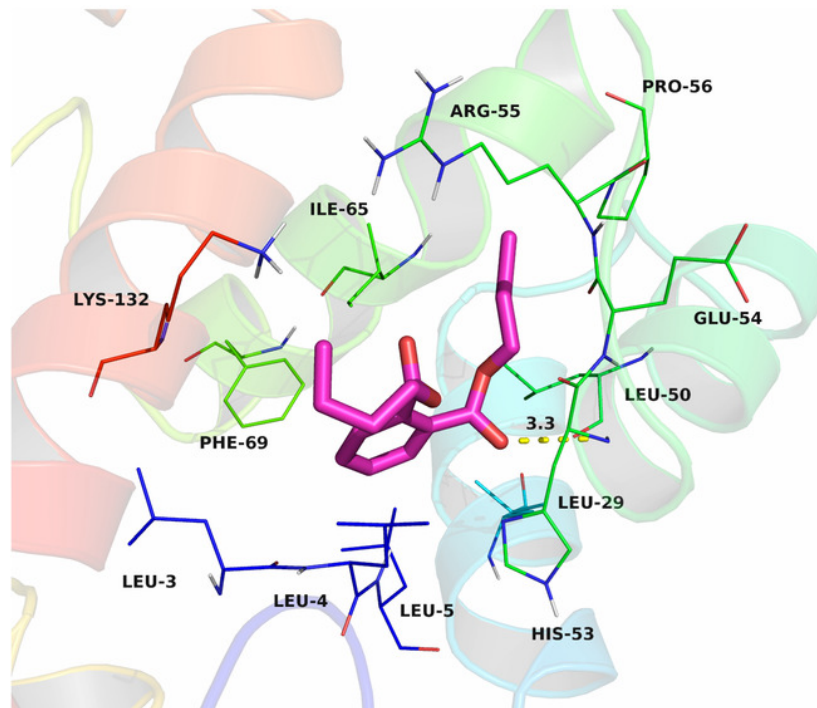


Figure 3

Double digestion map of the mutant and wild-type plasmids

Lane Marker: protein molecular weight standard; Lane 1: pET-28a (+)/PBP1-Phe69A; Lane 2: pET-28a (+)/PBP1-His53A; and Lane 3: pET-28a (+)/PBP1.

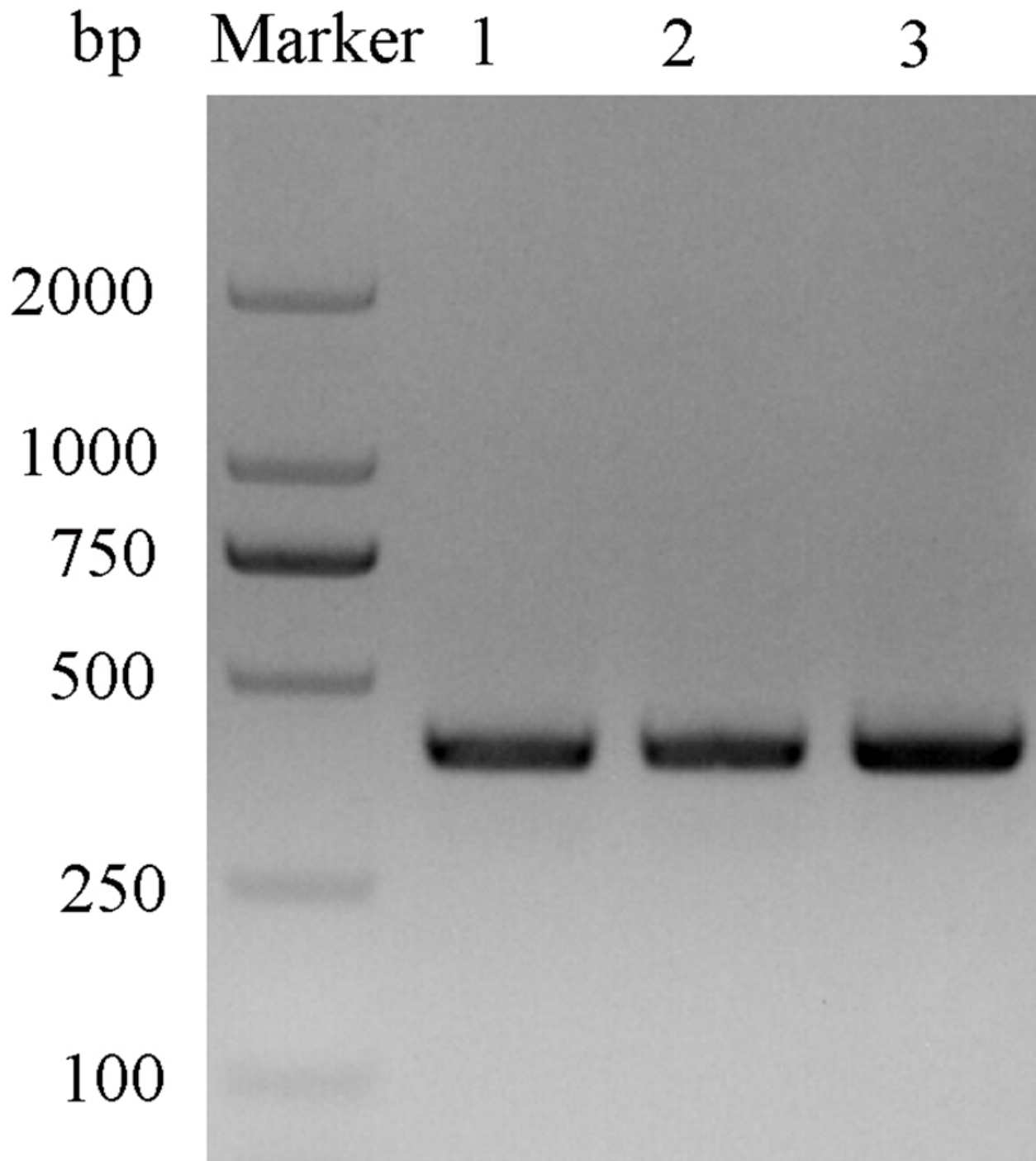


Figure 4

SDS-PAGE analysis of the total bacterial protein lysate of the mutant and wild-type CbuqPBP1

(A) CbuqPBP1-His53A mutant. Lane 1: IPTG induced total protein lysate; Lane 2: total protein lysate without IPTG induction. (B) CbuqPBP1- Phe69A mutant. Lane 1: total protein lysate without IPTG induction; Lane 2: IPTG induced total protein lysate. (C) wild-type CbuqPBP1. Lane 1: IPTG induced total protein lysate; Lane 2: total protein lysate without IPTG induction.

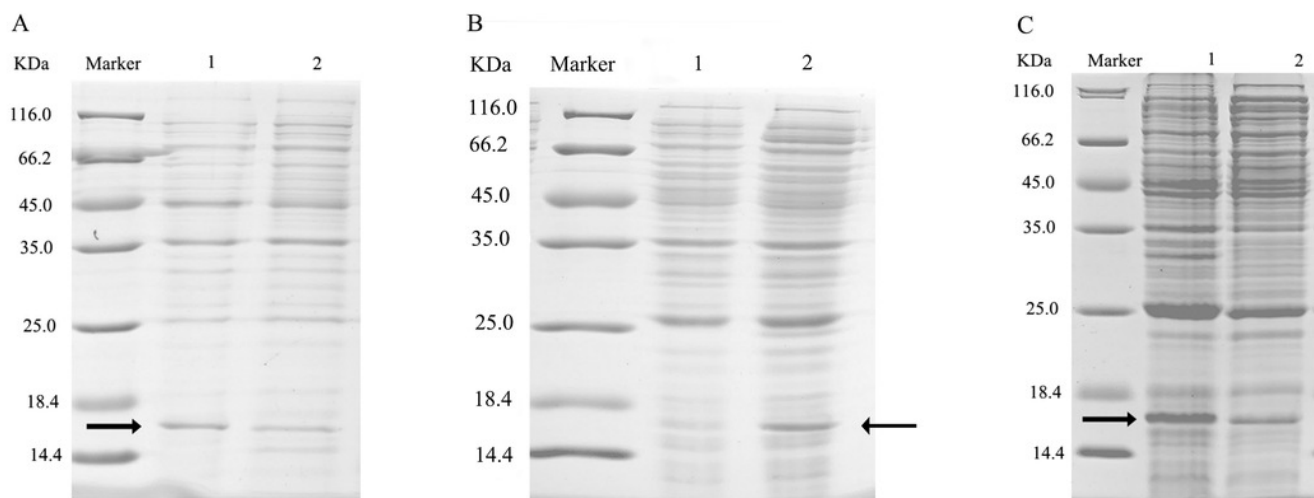


Figure 5

SDS-PAGE analysis of supernatant and precipitant of bacterial fragmentation following expression of the mutant and wild-type CbuqPBP1

Lane 1: IPTG induced expression of insoluble material; Lane 2: IPTG induced expression of supernatant following cell disruption by sonication. (A) wild-type protein. (B) CbuqPBP1-His53A mutant. (C) CbuqPBP1- Phe69A mutant.

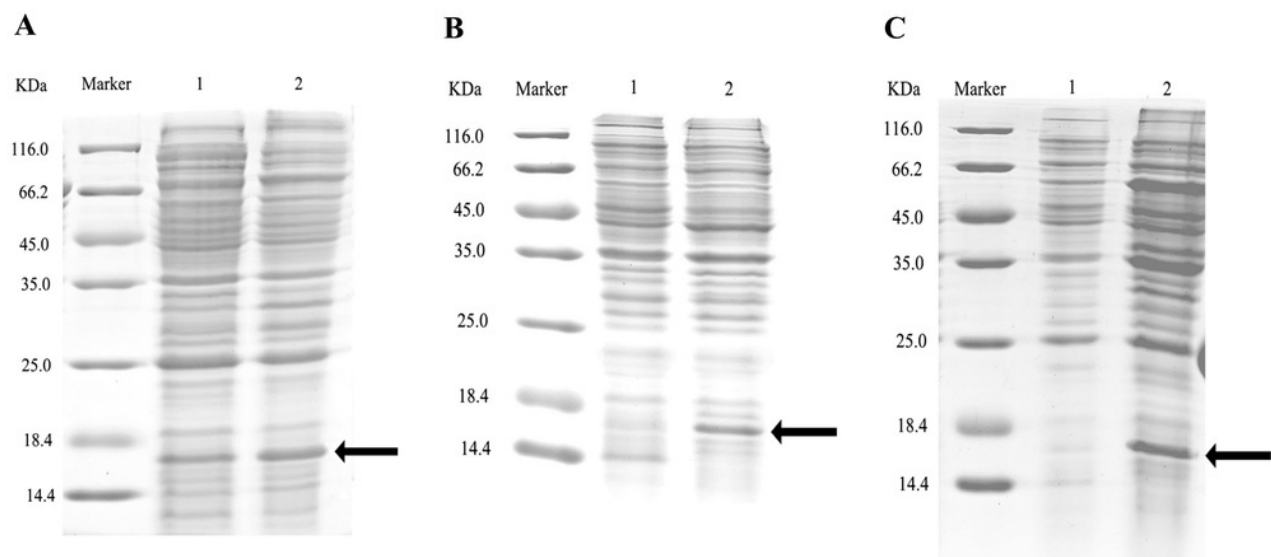
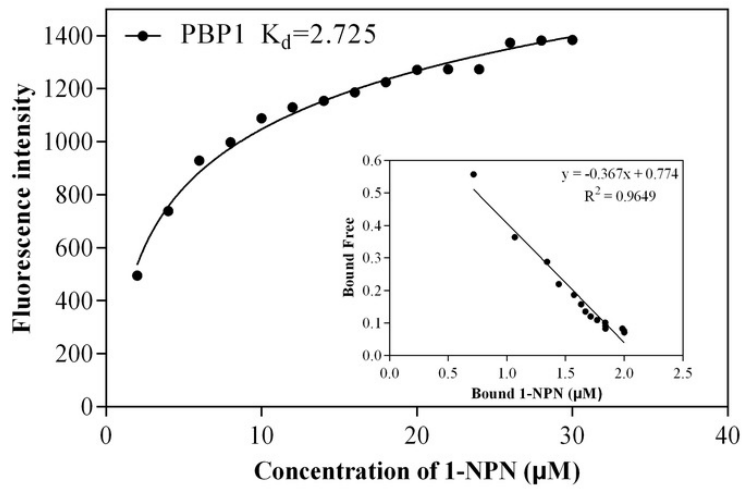


Figure 6

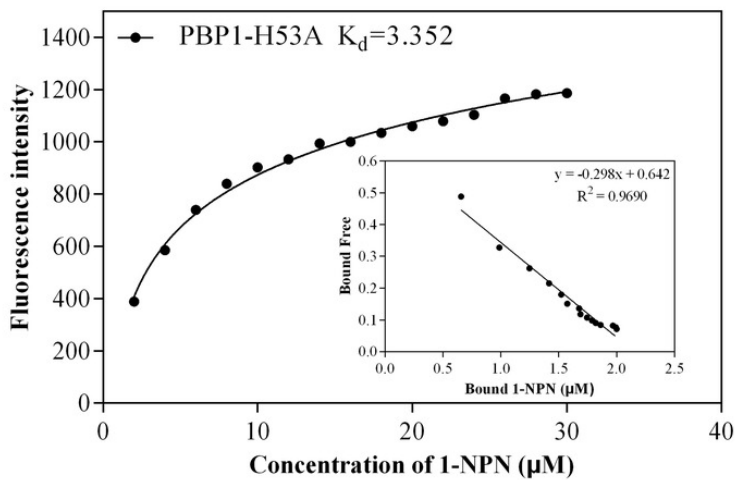
The binding curve and K_d of mutant and wild-type CbuqPBP1 toward 1-NPN

(A) wild-type protein. (B) CbuqPBP1-His53A mutant. (C) CbuqPBP1- Phe69A mutant.

A



B



C

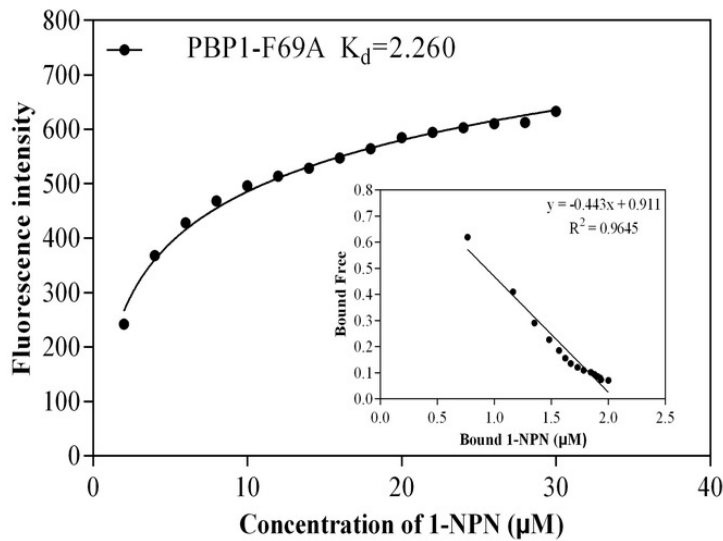


Figure 7

Competitive binding curves of selected ligands toward mutant and wild-type CbuqPBP1

(A) wild-type protein. (B) CbuqPBP1-His53A mutant. (C) CbuqPBP1- Phe69A mutant.

